Radiation Physics and Chemistry 211 (2023) 111043

Contents lists available at ScienceDirect

Radiation Physics and Chemistry

journal homepage: www.elsevier.com/locate/radphyschem

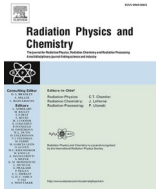

Comparison of methodologies for creating spread-out Bragg peaks in proton therapy using TOPAS and MCNP codes

I.S.L. Branco *, A.L. Burin, J.J.N. Pereira, P.T.D. Siqueira, J.M.B. Shorto, H. Yoriyaz

Centro de Engenharia Nuclear (CEENG), Instituto de Pesquisas Energéticas e Nucleares (IPEN), São Paulo, Brazil

ARTICLE INFO

Handling Editor: Dr. Chris Chantler

Keywords:
Spread-out bragg peak
Proton therapy
TOPAS
MCNP
Monte Carlo simulation

ABSTRACT

In proton beam treatments, the superposition of several weighted Bragg curves with different incident energies is required to homogeneously irradiate a large tumor volume, creating a spread-out Bragg peak (SOBP). This paper confirms on the suitability of two different methods to create SOBPs – Bortfeld/Jette's and MCMC (*Monte Carlo calculations and Matrix Computations*), using Monte Carlo simulations performed with TOPAS and MCNP6.1. To generate the SOBPs, algorithms were developed for implementation of the two methods, which enabled to find the weights for thirty variations of SOBPs, categorized according to their width and maximum depths. The MCMC method used weight optimization in designing SOBPs to avoid negative values. In contrast, the Bortfeld/Jette's method yielded the SOBPs according to the variation of a power-law parameter (p) introduced by the range-energy relationship. Optimal values of p, from MCNP and TOPAS, were selected in order to retrieve SOBPs with the best smoothness and then related to those obtained from the literature. In comparing both methods and codes, dose homogeneity parameters (*HOM*) were used to examine the SOBP flatness and gamma analyses were employed to assess the dose deposition along its full extension. The results showed that the SOBPs designed using the MCMC method had better *HOM* values and computational performance for both codes when compared to the Bortfeld/Jette's method. The gamma analyses highlighted significant differences between the entrance doses comparing the two different methods, for SOBPs with intermediate and high depths and small width. This evaluation was not possible with the *HOM* values alone, which stresses the relevance of a broad analysis to avoid unintended doses in healthy tissues.

1. Introduction

The adoption of accurate dose calculation and optimization techniques is of utmost importance for the efficacy of radiotherapy treatments, especially in all technology-driven modalities. In proton therapy, the three-dimensional relevance of dose distribution requires modulation of beam fluency in each field in both the perpendicular plane and in depth (Lomax, 1999) The modulation considers the unique physical properties of protons, including the Bragg Peak (BP), which is described by a sharp and narrow increase in dose deposition at a specific depth in tissue. The final form of BP is actually complex and relies on the beam energy spread and scattering components properties of the beam delivery system (Paganetti, 2018).

Due to the protons' dosimetric characteristics, a superposition of several peaks with different energies is required to obtain a homogeneous longitudinal distribution over a large tumor volume, creating a spread-out Bragg peak (SOBP). The simple addition of Bragg curves shifted in depth is not adequate to yield a uniform dose distribution, to do so, it is necessary to assign weights to each individual curve. Moreover, the extent of the SOBP can be adjusted, depending on the target size to be covered, by altering the number of added peaks and recalculating the assigned weights.

Passive scattering (PS) and uniform scanning (US) are two techniques commonly used in the field of proton therapy to deliver a uniform dose to the tumor. Both systems use SOBP as the fundamental element for in-depth dose delivery. An SOBP is typically produced by either a continuously rotating range modulator wheel or a ridge filter. The pattern of transverse dose distribution is a major distinguishing feature between these two systems. In PS, protons are scattered laterally to create a homogeneous intensity beam using single or double scatterers designed geometrically and in composition to produce a wide beam. In addition, field-specific apertures and range compensators conform the dose to the target (Paganetti, 2018). On the other hand, US utilizes a magnetic field to scan the proton beam, and, in this system, the beam

* Corresponding author.
E-mail address: isabela.slbranco@gmail.com (I.S.L. Branco).

https://doi.org/10.1016/j.radphyschem.2023.111043
Received 6 March 2023; Received in revised form 29 April 2023; Accepted 17 May 2023
Available online 27 May 2023

intensity remains constant and is swept over the transverse area of the treatment field of the patient in continuous scan line passes (James et al., 2018; Moskvin et al., 2015).

Regarding the applicability of the SOBPs research, in a recent paper, Yokokawa et al. (2019) proposed a new SOBP design method for low-energy regions, where the number of Bragg curves required to form the SOBP increases due to the sharpness of the peaks, and the range uncertainties greatly impact on the dose uniformity. They introduced a specially shaped mini ridge filter (MRF) to broaden the Bragg curves, reducing the required number of energy layers while keeping the distal falloff as sharp as possible. This simple system facilitates good dose uniformity and leads to higher efficiency of treatment time. Ghorbani et al. (2017) used MCNPX (Pelowitz, 2008) simulations to obtain Bragg curves that were weighted by an algorithm capable of solving a linear equations system. They investigated the differences between the SOBPs' characteristics in water and tissues with density close to water. The results pointed out that planning systems should include other parameters besides the electron density to perform the dose calculation more accurately.

Several other research papers have already addressed the problem concerning the production of SOBPs, in particular, the ones by Bortfeld and Schlegel (1996), Gardey et al. (1999), Pedroni et al. (2005), Hérault et al. (2007, 2005), Jette and Chen (2011), Rezaee (2018), and Velten and Tomé (2020). A number of them thoroughly describe the SOBPs algorithms used to weight the Bragg curves. Bortfeld and Schlegel derived a simple analytical approximation for the depth–dose distribution of SOBP proton beams. Jette and Chen modified the former analytical expressions and arbitrarily varied the recommended power law parameter (p) therein, which relates the proton range to its energy, and succeeded in creating satisfyingly uniform SOBPs using MCNPX. Posteriorly, Velten and Tomé performed simulations with TOPAS time features (Perl et al., 2012) and, when using Jette and Chen power law parameter, they were unable to reproduce the flat SOBPs. Hence, they investigated new different optimal values for p. In contrast to those methods, Rezaee used simulated Bragg curves, for oxygen ion beams, to introduce a numerical method that relates Monte Carlo calculations and Matrix Computations (MCMC). This method allowed the yield of smooth SOBPs, which were later compared to those produced with Jette and Chen's analytical model.

The development of dose optimization algorithms is characterized as a solution that allows comparing the influence of different mathematical models in the treatment efficiency. In particular, SOBP algorithms enable the observation of how different models distribute doses across the entire depth extension of the tumor, thereby ensuring that the tumor is uniformly irradiated and preventing the presence of hot or cold dose spots. A commercial system cannot perform such a comprehensive analysis of the influence of mathematical models because users cannot access or modify all parameters used in the dose calculations. In this scenario, the present study reports on the suitability of two algorithms with different methods for creating protons SOBPs – Bortfeld/Jette's and MCMC. Dose uniformity was achieved using weighted Bragg curves obtained from simulations performed with two Monte Calo (MC) codes: TOPAS and MCNP6.1 (Pelowitz, 2013).

The comparison of two different Monte Carlo codes permits observation of their respective approaches to the same problem to verify whether the codes correctly simulate the physics of the system. In this study, the default parameters of both codes were maintained to ensure that there was no significant modification to the physics in the simulations. Our findings indicate that TOPAS and MCNP show good agreement, with a relative difference of about 2% between the ranges of the two codes (see section 3.1). Moreover, comparing the performance of different codes allows the optimization of computational resources. Since MCNP6.1 is unable to run multi-threaded simulations with its built-in code features when using a proton source, TOPAS produced faster simulations, making it more suitable for real clinical case studies that require time-saving treatment solutions. Lastly, when experimental measurements are unfeasible, the comparison of two Monte Carlo codes is imperative to confirm the validity of the simulation results and ascertain information regarding the sources of error and potential biases.

In analog mode, the analysis of two different algorithms of dose optimization methods is essential to evaluate their performance, accuracy, and reliability in radiation dose estimation. Therefore, initially in this study, by deriving the dosimetric parameters from the range-energy relationship (α and p - explained in section 2.4), we were able to calculate the Bragg curves weights according to the Bortfeld/Jette's formulas. The variation of the p-value served as a basis for the analysis of the SOBPs flatness, comparing the different MC codes results and also, the values previously reported in the literature. The second method in this study, MCMC, did not require the variation of parameters related to the weight calculation, it only used the Bragg curves to design the SOBPs and discarded possible negative weight values.

The purpose of the present study is to assess two different methods for calculating the weights of SOBPs, similarly outlined by Rezaee, and to estimate the differences between the dose deposition predictions of SOBPs from MC simulations using MCNP and TOPAS codes. The developed algorithms are described in detail using flowcharts to provide the reader with comprehensive insight into both methods and their various components. It is intended that the simplicity and easy implementation of the algorithms can potentially act as inspiration for the development of new applications, thereby contributing to knowledge advancement within the field. This paper also includes the energy-range relationship curves for each MC code, which are not commonly reported in related studies. These curves confirm that the obtained α and p parameters are consistent with the ones described in reference literature, supporting the physics used in the simulations. A set of p-optimal parameters was also provided to obtain different widths and depths of flat SOBPs in water using the TOPAS and MCNP codes, highlighting the difference between these codes and p-optimal values presented in the literature. Apart from comparing MC simulations and SOBP methods, this study evaluated the results using two parameters: dose homogeneity (HOM) and gamma analysis. The first analyses the plateau of the proton SOBP, and the latter assesses the dose deposition in the SOBP full extension, which is not broadly discussed in papers presenting methods to create SOBPs despite its common use in clinical practice. The inclusion of gamma analysis stressed the relevance of a broad dose evaluation to avoid unintentional ones in healthy tissue, especially concerning the entrance doses.

2. Materials and methods

2.1. Monte Carlo codes

Two MC codes were used to calculate the energy deposition that arises from monoenergetic proton beams in this study: TOPAS (Perl et al., 2012) and MCNP (Pelowitz, 2013). In simulations with both codes, the geometry and the scoring volumes were identical, and they were performed with as many default physics parameters as possible. These descriptions are presented in the following sections.

2.2. TOPAS

TOPAS (Perl et al., 2012) (version: 3.7.0) is an application, written in C++ language, that extends the tools used by the Monte Carlo code GEANT4 (Agostinelli et al., 2003; Allison et al., 2016) (version 10.06. p03) to simulate radiation transport. Thus, TOPAS relies on the same physical models, processes, and interaction cross sections present in GEANT4.

TOPAS default physics list was defined based on extensive validation of the code against experimental measurements for proton therapy and were therefore used in all simulations (Testa et al., 2013, 2014). That list employs *g4em-standard_opt4* for electromagnetic physics, *g4decay* for

radioactive decay processes of all long-lived nuclei, *g4h-elastic_HP* for elastic scattering of hadrons, *g4h-phy_QGSP_BIC_HP* for nuclear interactions using Binary Intranuclear Cascade (BIC) Model, *g4ion-binarycascade* for nuclear interactions using binary cascade for light ions, and *g4stopping* to provide the nuclear capture of negatively charged particles at rest (Jarlskog and Paganetti, 2008).

The default physics list includes models that can handle the transport of protons and various secondary particles such as neutrons, electrons, tritons, photons, alphas, etc., through matter. The simulations used only proton beams as a source but had no restrictions on the types of particles that were scored.

The output files from the TOPAS simulations provided data from the *EnergyDeposit* scorer, which tallies the sum of all deposited energies in a given volume in MeV.particle^{-1} units, from all particle types.

2.3. MCNP

MCNP is a general-purpose radiation-transport code, written in Fortran and C, and based on the MC method, which enables, in its version 6.1 (Pelowitz, 2013), multigroup/adjoint transport of protons, neutrons, photons, and electrons, among other particles, over broad ranges of energies.

MCNP6.1 is not capable of running multi-threaded simulations involving heavy charged particles (Zieb et al., 2018). It is worth noting that in the radiotherapy community, the term "heavy charged particles" is not generally used to refer to protons, in contrast to MCNP. Instead, this term is commonly used to describe ions, such as carbon or oxygen.

As the built-in code features of MCNP6.1 do not provide a prompt solution to parallelizing simulations, when using a proton source, a viable solution could be implemented by generating multiple simulations with distinct seeds, which will produce varied results. These results can subsequently be combined into one through the use of in-house scripts. In this study, while it was possible to manually parallelize simulations to increase the number of particle histories, no major statistical errors related to the simulations were detected. The code's built-in functionality was instead utilized to transport primary and secondary protons (identified by the symbol H), as well as neutrons (N), photons (P), electrons (E), and heavy ions (#).

Default physics parameters were kept, but, for protons, the upper energy limit for transport was set to 250 MeV in all simulations. Also, table-based physics was enabled, so physics models were used for energies above 10^{-3} MeV and data tables for those below this value. Light ion recoil control from elastic scattering was set to 0.5 and the stopping power energy spacing (*efac*) was set to 0.99 to increase the sampled points in multiple-scattering tables, yielding smoother Bragg curves. The only parameters changed in neutron physics was light-ion and heavy-ion recoil and NCIA control (*coilf*) that was set to 1.5, and table-based physics cutoff, which uses physics models for energies above 10^{-3} MeV and data tables for lower energies. In photon physics, Doppler energy broadening was disabled and, for all other particles transported, the physical parameters were identical to the default.

The requested libraries provide validated data of cross-section interactions, whether they are based on measurements or nuclear models. Those adopted in the simulations were *endf70* (70 h) for protons and *endf60* (60c) for neutrons.

The results were tallied in MCNP using *tmesh tally type 3*, which scores the energy deposited per volume (in units of MeV.cm^{-3}.particle^{-1}) coming from all primary and secondary particles tracked in the problem. This defined virtual mesh had the same dimensions as the scored volumes in the simulations performed with TOPAS.

2.4. Simulations settings

The phantom geometry designed in simulations is shown in Fig. 1. The outside world is a vacuum cube with dimensions 3.0 × 3.0 × 3.0 m^3 and the phantom in it has a rectangular shape of 20.0 cm at each side (x and y) and length (z_{total}) of 40.0 cm. This phantom was filled entirely by water and divided into slices in the z direction (Δz), with thicknesses of 0.01 cm for energies less than or equal to 100 MeV and 0.05 cm for the other energies between 100 MeV and 250 MeV. The radiation source for all simulations was a flat cylindrical beam (0.2 cm radius) of monoenergetic protons with no angular divergence. Proton pencil beam, along the z -axis, travels 5.0 cm (denoted as SSD in Fig. 1) until it hits the anterior face of the phantom.

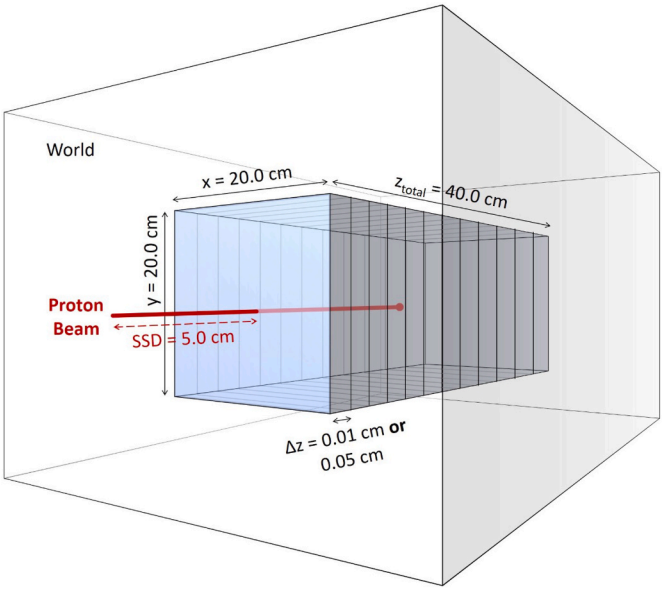

Fig. 1. Schematic representation of the geometry used in TOPAS and MCNP simulations (not to scale). A monoenergetic proton beam impinges on a water phantom coming from a vacuum medium. The deposited energy was computed in all z-axis bins.

In order to evaluate the depth-dose distribution in the beam axial direction, the results were scored in each mesh bin set, i.e., with dimensions of 20.0 × 20.0 x Δz cm^3. TOPAS scored the results on a mesh defined in the simulation geometry itself, while the mesh used in MCNP was virtual, but both had identical bin volumes according to the incident energy. It is important to recognize that alternative simulation geometries, such as positioning the proton source further from the phantom and in air, may yield wider Bragg peaks owing to the intrinsic divergence from the beamlets. However, this occurrence does not hinder the exploration of SOBP optimization techniques. Rather, it emphasizes the necessity of having a sufficient distance between the peaks to prevent undue overlap. Similarly, it is feasible for the proton source to possess dimensions within a few centimeters, given that there is a sufficiently sizable area scorer to measure the accumulated dose on the slices. The selection of monoenergetic beams and general geometry outlined in this study was a deliberate choice made to facilitate accurate comparisons with existing literature.

Two example sets of normalized depth-dose distributions are shown in Fig. 2, each containing 11 pristine Bragg curves spaced by 2 MeV increments. The first has a minimum energy of 80 MeV and a maximum of 100 MeV, which define the Bragg peaks at positions $z = 5.15$ cm and $z = 7.66$ cm. In the second set, the Bragg peaks extend from $z = 10.58$ cm to $z = 13.88$ cm, corresponding to 120 MeV and 140 MeV, respectively. Considering both sets, it is possible to observe clearly how the energy straggling effect acts on the Bragg peak widths due to statistical variations in the proton energy loss, causing a spread in the energy distribution, which makes the peaks narrow for lower energies and thicker for higher ones (Newhauser and Zhang, 2015; Paganetti, 2018; Sawakuchi et al., 2008).

As an example, the total doses, calculated by summing all 11 pristine Bragg curves, are also shown in Fig. **2**. Both sums do not have the

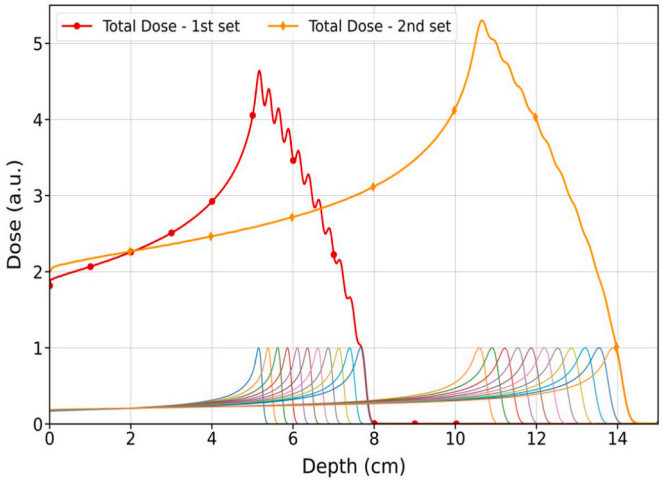

Fig. 2. Proton depth-dose profiles for different incident energies split into two sets with 11 curves each. The total dose for each set, calculated as a sum of the curves, is also presented still without the weight factors that feature a homogeneous SOBP.

necessary flatness requested by the SOBP, so it is mandatory to assign weights that modify the intensity of each curve. Even disregarding the weight factors that should be assigned, it is possible to predict that the first set in the graph will present more dose fluctuations regions due to the narrower peaks, directly impacting the SOBPs' smoothness. To address this issue, in this study, 21 distinct incident proton energies were adopted for each SOBP, so that adequate homogeneity was possible while avoiding large gaps between the peaks.

In the light of these considerations needed to build a SOBP, the simulations were divided into two main steps. In the first step, raw data, extracted from the MCNP and TOPAS simulations outputs, were used to establish a correlation between the incident energy and the range position of each beam, referred to as the range-energy relationship (detailed in the following section 2.4). For that, incident energies ranging from 20 MeV to 250 MeV, spaced in 2 MeV increments were considered, leading to 232 simulations for each code.

In the second step, simulations were partitioned into 30 groups. The reason behind this was that, as done by Jette and Chen (2011) and, Velten and Tomé (2020), SOBPs were built for five maximum depths, i.e., with five maximum proton energies (E_0 = 50 MeV, 100 MeV, 150 MeV, 200 MeV, and 250 MeV); for each of these energies, six widths of SOBPs were assigned (χ = 15%, 20%, 25%, 30%, 35%, and 40%). The widths of SOBPs (χ) are conventionally defined in the literature as a percentage of the range (R_0) of the highest energy peak (E_0) that composes it. Therefore, in case a SOBP had to be designed with a width of 6.0 cm, with its highest energy having a range of $R_0 = 20$ cm, χ would be 30% and the SOBP would extend from the depth $(1-\chi).R_0$ (in the example: $(1\ \ 0.3)\ .\ 20 = 14$ cm) to the depth R_0.

In addition, the second step used the correlation between range and energy, obtained in the first one, to establish the incident energies needed to compose the simulations. Altogether, 770 simulations (from TOPAS and MCNP) were generated and analyzed, which allowed the SOBP weighting factor to be controlled and easily modified by script written in Python programming language (Rossum, 1995).

2.5. Data analysis

To assess and compare the flatness of the distinct SOBPs, we used the dose homogeneity parameter (referred to as *HOM*) described by Rezaee (2018). This parameter can be defined as the ratio between the lowest and the highest dose calculated within 80% of the SOBP, i.e., between the points from $(1-0.9\chi).R_0$ to $(1-0.1\chi).R_0$. Gamma analysis was also used to compare the differences in results for all codes and methods, since it can evaluate the entire longitudinal dose profile and not only the SOBP plateau as *HOM* does.

Reference indices have been adopted along this paper to designate the analyzed set of data according to method and code used to produce them. The indexes and the names of the corresponding sets are presented in Table 1. The details of both methods used as well as their parameters will be explained in the following sections.

2.6. Bortfeld and Jette's method

In their paper, Bortfeld and Schlegel (1996) introduce an analytical expression for weighing individual Bragg peaks as a function of range, which is essential for creating a SOBP with the desired width and depth. Such an analytical approach was derived from the single assumption that the range of a proton beam can be directly related to its initial energy and the medium where the transport of radiation occurs. A simple power law, known as range-energy relationship (Bortfeld, 1997; Newhauser and Zhang, 2015), can be used to describe this relationship, as given by:

$$\mathrm{R(E)} = \alpha E^{\mathrm{p}} \tag{1}$$

In Eq. 1, $R(E)$ is the proton range, E is the initial energy of the proton beam and the exponent p is an energy-dependent parameter (dimensionless). For energies up to 10 MeV, this relationship is known as Geiger's rule and has $p = 1.5$. For proton in therapeutic beam energies the exponent becomes $p \approx 1.7$–1.8 (Evans, 1955; Ulmer, 2007). Moreover, in Eq. 1, the parameter α, given in cm/MeV$^{\mathrm{p}}$, is a material-dependent constant since it is inversely proportional to the mass density of the medium (Bortfeld, 1997).

In 2011, Jette and Chen modified the analytical model proposed by Bortfeld and Schlegel in order to improve the flatness of the SOBP. To this end, they considered that the SOBP need to be divided into n equal intervals and the range of monoenergetic beams has to correspond to the depth of the ends of these intervals. Thus, the intervals employed are:

$$r_k = \left[1 - \left(1 - \frac{k}{n}\right)\chi\right].R_0 \tag{2}$$

Where R_0 is the range of the highest energy peak; χ is a percentage of that range, which corresponds to the width of the SOBP; n is the number of energy intervals (the total number of beams is equal to $n+1$, and, in

Table 1
Reference indices used to represent each dataset, sorted according to the method and code used.

Reference Index	Method and Codes used in the Dataset
$\mathrm{Jette_{T\text{-}org}}$	Simulations performed with the TOPAS code that used Bortfeld and Jette's method to calculate the SOBPs weights (w), with original p-value ($p = 1.75$).
$\mathrm{Jette_{M\text{-}org}}$	Simulations performed with the MCNP code that used Bortfeld and Jette's method to calculate the SOBPs weights (w), with original p-value ($p = 1.75$).
$\mathrm{Jette_{T\text{-}opt}}$	Simulations performed with the TOPAS code that used Bortfeld and Jette's method to calculate the SOBPs weights (w), with optimal p-value.
$\mathrm{Jette_{M\text{-}opt}}$	Simulations performed with the MCNP code that used Bortfeld and Jette's method to calculate the SOBPs weights (w), with optimal p-value.
$\mathrm{Jette_{M\text{-}Tw\text{-}org}}$	Simulations performed with the MCNP code that used the weights obtained in $\mathrm{Jette_{T\text{-}org}}$ to calculate the SOBP.
$\mathrm{Jette_{M\text{-}Tw\text{-}op}}$	imulations performed with the MCNP code that used the weights obtained in $\mathrm{Jette_{T\text{-}opt}}$ to calculate the SOBP.
$\mathrm{MCMC_T}$	Simulations performed with the TOPAS code that used MCMC's method to calculate the SOBPs weights (w).
$\mathrm{MCMC_M}$	Simulations performed with the MCNP code that used MCMC's method to calculate the SOBPs weights (w).
$\mathrm{MCMC_{M\text{-}Tw}}$	Simulations performed with the MCNP code that used the weights obtained in $\mathrm{MCMC_T}$ to calculate the SOBP.

this paper, $n = 20$) and k is the k-th beamlet that will be used to build the SOBP, so $k = (0, 1, 2, \ldots, n)$.

In this study, once the r_k values were calculated, a linear interpolation was done to obtain the energies corresponding to that range (E_k), using data from the TOPAS simulation as a reference. Subsequently the weights of proton beams with several initial energies were computed by the following formulas:

$$w_k = \begin{cases} 1 - \left(1 - \dfrac{1}{2n}\right)^{1-p^{-1}} & \\ \left[1 - \dfrac{1}{n}\left(k - \dfrac{1}{2}\right)\right]^{1-p^{-1}} - \left[1 - \dfrac{1}{n}\left(k + \dfrac{1}{2}\right)\right]^{1-p^{-1}} & k = 1, 2, \ldots, (n-1) \\ \left(\dfrac{1}{2n}\right)^{1-p^{-1}} & k = n \end{cases} \quad (3)$$

The parameters exhibited in Eq. 3 are the same as those in Eq. 1 and 2.

Several studies have shown that setting a single p-value can produce SOBPs with non-optimal flatness and smoothness even when applied to a single particle type (Jette and Chen, 2011; Rezaee, 2018; Velten and Tomé, 2020). When varying the p -parameter to design an SOBP with the desired width and depth, it is possible to establish a value that achieves adequate dose homogeneity in its plateau. Therefore, it is challenging to develop a single way to set a p-value that could be incorporated into treatment planning systems.

In this paper, the presented method will be referred only as Jette's method for convenience. As mentioned in a previous section, it was used to create thirty SOBPs with distinct depths and widths by both MC codes. For each one of these groups of SOBPs, the p-value varied from 1.2 to 2.0 in 0.01 steps, changing the weights assigned to the pristine Bragg curves (according to Eq. 3) and allowing the selection of an optimal p-value that would produce the most uniform SOBP for that group.

The flowchart shown in Fig. 3 outlines the details of the algorithm developed for the Jette method, mainly highlighting the procedure for varying the p-parameter, and how the optimal p-value was chosen according to the *HOM* parameter. In addition, the weights, the SOBP curve and the *HOM* generated through the original value of p (the one obtained by the first group of simulation runs - section 2.2) were stored for later comparisons.

2.7. MCMC method

Rezaee's (2018) introduces a numerical method for computing the weights of the Bragg curves to compose an SOBP. This numerical method is a combination of MC calculations and matrix computations and is called MCMC method.

The MCMC method states that to define appropriate weights, it is first necessary to create a matrix D. This matrix D is square, with dimensions $(n + 1) \times (n + 1)$, and it considers only the points within the SOBP width. Here, n is still the number of energy intervals. The elements in D, represented by $D_{k,i}$ refer to the amount of dose delivered by the beam with energy E_i, at point r_k. The r_k points are the exact locations of the Bragg peaks obtained from MC simulations. Fig. 4 illustrates the assigned values for some elements in D.

In this present study, the outputs from the simulations were inserted into a given matrix M, containing the data from the 21 pristine Bragg curves, with dimensions $(z_{total}/\Delta z)x21$, where $z_{total}/\Delta z$ rows correspond to the longitudinal dose profile slices which make up the calculated Bragg peak curve. In this paper, matrix M assumed dimensions of $(4000x21)$ for energies less than or equal to 100 MeV and $(800x21)$ for the other energies between 100 MeV and 250 MeV. Thus, the matrix D was directly extracted from M because the selected rows in M corresponded to the positions of all Bragg peaks.

The MCMC method has been slightly adapted in this study, but like in other studies (Gardey et al., 1999; Golub and Reinsch, 1971), it attempts to solve the equation:

$$\mathrm{D} \times \mathrm{w} = \mathrm{dmax} \quad (4)$$

Where D is the matrix previously explained in this section, w is a vector containing the beam weights and *dmax* is a vector representing the prescription dose. Eq. 4 addresses the matrix form of the problem that can also be represented by the following linear equations, generated at all points in the depth r_k where there is a BP:

$$\begin{cases} D_{0,0}w_0 + D_{0,1}w_1 + D_{0,2}w_2 + \ldots + D_{0,n}w_n = 1 \\ D_{1,0}w_0 + D_{1,1}w_1 + D_{1,2}w_2 + \ldots + D_{1,n}w_n = 1 \\ D_{2,0}w_0 + D_{2,1}w_1 + D_{2,2}w_2 + \ldots + D_{2,n}w_n = 1 \\ \qquad\qquad \ldots \\ D_{n,0}w_0 + D_{n,1}w_1 + D_{n,2}w_2 + \ldots + D_{n,n}w_n = 1 \end{cases} \quad (5)$$

In Eq. 5, the dmax values appears to be equal to 1 for all equations, as initially adopted for this study, corresponding to a SOBP plateau of 100%. In order to find the beam weight values we need to solve Eq. 4, so that:

$$\mathrm{w} = D^{-1} \times \mathrm{dmax} \quad (6)$$

As can be seen in Eq. 6, the issue in determining the beam weights is that one must find the inverse of the matrix D. This system could generate negative values of w. Since negative weight values cannot be delivered, weights and the corresponding curves must be removed and then the optimization is recalculated.

The flowchart shown in Fig. 5 outlines the details of the algorithm developed for the MCMC method, highlighting mainly the procedure for excluding the curves with negative weights. The algorithm is designed to keep the weights of the highest and lowest energy BP curves always positive to ensure that the width defined for the SOBP is satisfied. Also, the weights, the SOBP curve, and the calculated *HOM* were stored for later comparisons.

3. Results and discussion

3.1. Parameters from the range-energy relationship

In the simulations, every pristine Bragg curve presented a statistical error for the calculated doses, inherent to the MC method. As the proton fluence decreases along its trajectory and undergoes a sharp fall near the end of the range, the number of particle interactions also drops after this region, increasing the statistical error according to the law of large numbers. For this reason, in this paper, the statistical uncertainties were evaluated until the $R_{0.5}$ point, i.e., where the dose is equal to 0.5% of its maximum value.

In the first simulations step, regarding the MCNP code, the error value was not greater than 2.0% in all extension of the curves until the $R_{0.5}$ point, and for TOPAS, the maximum error up to the same point was 1.96%. When considering the doses at the Bragg peaks, the maximum errors were approximately 0.13% for both codes. The error values were considered small enough, ensuring the accuracy of the estimated quantities and their locations in the geometry of interest.

Fig. 6 shows the correlation between the proton beam's incident energy and its range position.The simulation data, from both codes, were used to fit curves described by Eq. 1 through the method of nonlinear least squares, according to the Levenberg-Marquardt (LM) algorithm already implemented in Python (Rossum, 1995) by *SciPy* package (Virtanen et al., 2020).

Along with the fits in Fig. 6, the values and uncertainties of the α and p parameters obtained are presented. To obtain such parameters through the LM algorithm, standard deviations were assigned to the depth points as being half the value of their bins, i.e. $\sigma_z = 5.0 \times 10^{-3}$ cm for energies less than or equal to 100 MeV and $\sigma_z = 2.5 \times 10^{-2}$ cm for all other energies higher than 100 MeV. The parameters values were very similar for

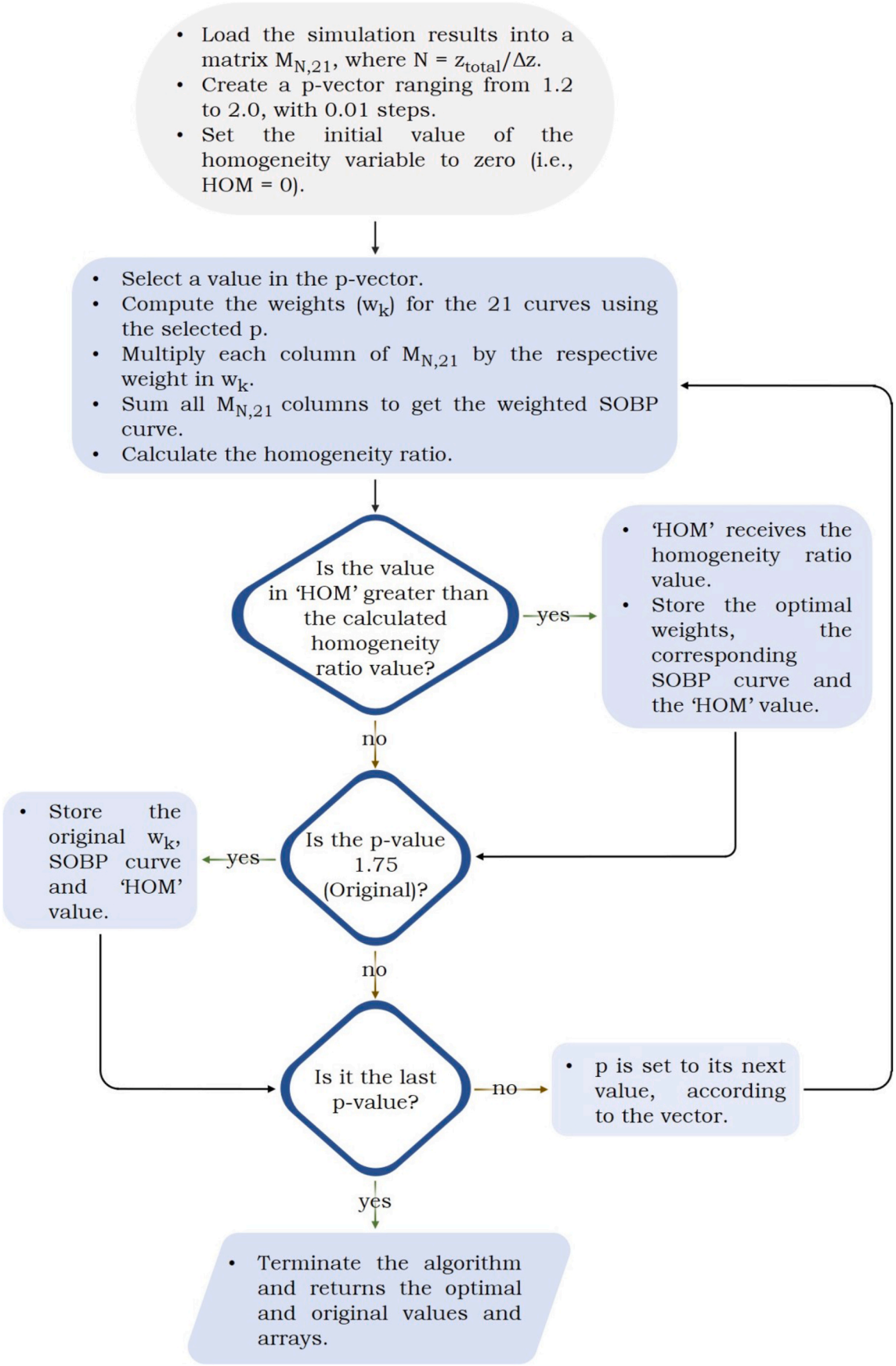

Fig. 3. Flowchart describing the steps involved in the implemented algorithm for weights calculation, variation of the *p* parameter, acquisition of the homogeneity ratio (*HOM*) and the SOBP curve for Jette's method.

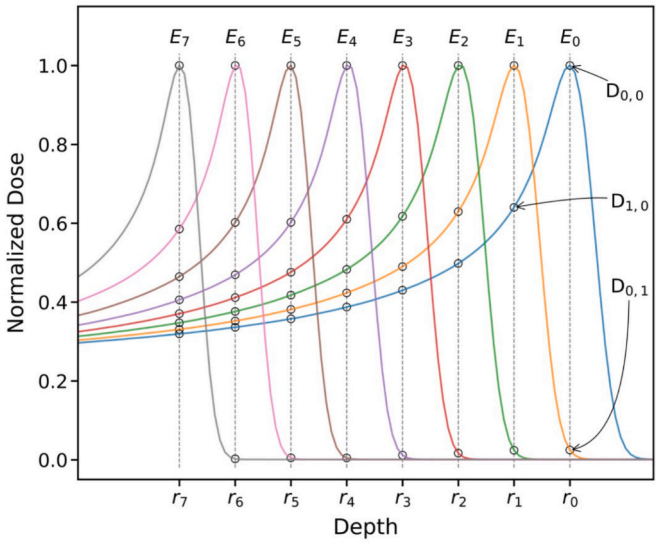

Fig. 4. Schematic of some of the points corresponding to the elements in matrix *D*, necessary for the weight's calculation in the MCMC method.

both MC codes and also when compared to those reported by Bortfeld (1997). From the acquired p (simulated data), even considering its uncertainties, an original value could be defined as 1.75, which was used to observe the differences between the *HOM* with this fixed and initial p and with variable ones.

In the bottom graph of Fig. 6 is shown the relative difference between the MCNP and TOPAS data for all energies, the latter code being adopted as reference for having been validated with experimental measurements (Testa et al., 2013, 2014). The largest relative differences occurred for the points with lower energies and still had values approximately around 2%, indicating good agreement between the ranges for the two codes. Similarly, by comparing the simulated data from both codes with those from Bortfeld's, relative differences of up to 3.1% were found for the lower energies and about 2.3% for the higher ones (data not shown).

In addition to the range analyses, maximum-to-plateau ratios were calculated for both MCNP and TOPAS (data not shown). As the name implies, the ratio was established using the maximum dose from the Bragg curve and the average dose at points characterizing the entrance dose plateau. This average was done with the initial points going up to 10% of the BP distance; for instance, for the energy of 100 MeV with the BP at 7.66 cm, the average dose was calculated from the points corresponding to 0 cm up to 0.76 cm.

After obtaining the maximum-to-plateau ratio for both codes at all energies, the relative differences between them were calculated (data not shown). The results that exhibited higher relative differences were present at lower energies; at 30 MeV, this value reached 10%, which was the maximum value found. However, the overall mean relative difference was approximately 0.5%. The differences for low energies could potentially be associated with the radiation transport of each code, as the propagated statistical errors of the ratios reached only 0.7%.

From the simulated TOPAS data, the ranges for the simulations in the second step were determined using Eq. 2, and a linear interpolation was done to calculate the energies matching this range. Thus, the TOPAS and MCNP simulations used the same set of incident energies to compose the 30 groups of SOBPs.

3.2. Spread-out Bragg peaks

In the second simulations step, the analysis of all the pristine Bragg curves that composed the SOBPs using the TOPAS code led to a maximum error of 0.83% up to the $R_{0.5}$ point, and for MCNP this value was 1.28%. As expected, the maximum errors in the Bragg peaks were smaller, standing at 0.06% and 0.08% for TOPAS and MCNP respectively. The errors found were considered acceptable for designing SOBPs with sufficient accuracy.

Simulations in the second step branched into several groups for each MC code, based on the highest incident energy (E_0) and width (χ) of the SOBPs, as represented in Fig. 7. In the same figure, it is possible to notice the SOBPs yielded when the MCMC method and Jette's method were applied, with the latter alternating the p -value chosen between optimal and original to weight the pristine Bragg curves. All the SOBPs shown were normalized by their corresponding value at middle point, i.e., at $(1 - 0.5\chi).R_0$, and then multiplied by arbitrary constants to avoid overlap between SOBP curves with different widths (χ).

The MCMC method achieved suitable results for the coverage and flatness at the required widths for both codes. The Jette's method with p-optimal reveals a coverage gap at the SOBPs extremes for low E_0, especially when the wider ones are analyzed. As the E_0 increases the inverse behavior is perceived, the dose increases at the extremes relative to the middle of the SOBPs. This small dip for high energies was also reported in the paper by Jette and Chen (2011) and Velten and Tomé (2020).

In the curves of Jette's method with p-original, for both MCNP and TOPAS codes, it is notable that the SOBP appears tilted specially for higher E_0 and larger widths. This tilt was also described in Jette's study and happens mainly because their analytical formulas for weighting the Bragg curves were derived from Bortfeld and Schlegel (1996), which initially did not consider the range straggling effect in proton beams.

The correct dose estimation at the edges of the SOBP is primarily important to avoid unneeded radiation dose to healthy tissue, and, flatness in its extent ensures that the entire tumor will be irradiated homogeneously. In addition to the dose comparisons, both methods also differed in their computational performance. The time for running the algorithm concerning the Jette's method was around hundredths of a second for each one of the 30 groups, but even so, because of the change in its p-parameter, this time was up to about 29 times longer than the one for the MCMC method for both codes.

3.3. Variations in the p-parameter

The suggestion to vary the p-parameter to produce a flatter and more homogeneous SOBP was first made by Jette and Chen (2011) to adjust its tilt due to the effect of energy straggling on dose deposition. As it was done in the aforementioned study, this paper adopted 0.01 steps between the analyzed p-values, and the maximum and minimum edges (2.0 and 1.2) were also based on the values already published by Jette and Velten and Tomé (2020).

In Fig. 8 the dose homogeneity parameter of the resulting SOBPs (*HOM*) can be seen according to the p-value variation applied in the Jette's weighting formulas. The point where each curve has a peak shows the highest *HOM* value, where the most appropriated p-value stands out. The original p-value (1.75), obtained with the first step of simulation runs, is indicated in all graphs by a black dotted line. The plots were also categorized according to the maximum energy among the incident beams composing the SOBP (E_0), SOBP width (χ) and MC codes used in the simulations.

In Fig. 8 graphs, it can be firstly observed that the *HOM* values derived from the change of p presented similar behavior when TOPAS and MCNP simulations were used. For lower E_0 analyzed, in general, the highest *HOM* occurred when p-values were close to 1.75. For 50 MeV, the p-optimal for large widths of SOBPs start to diverge from the original one, which is also true for small widths at 100 MeV. In addition, as the E_0 increase, the p-optimal values decrease broadly for all SOBP widths. Table 2 summarizes the information in Fig. 8 and shows all p-optimal values defined according to the algorithm developed in this study, for both MCNP and TOPAS.

The data from Table 2 confirm that the variation of the p parameter produced similar *HOM* values between the two codes since the p-optimal

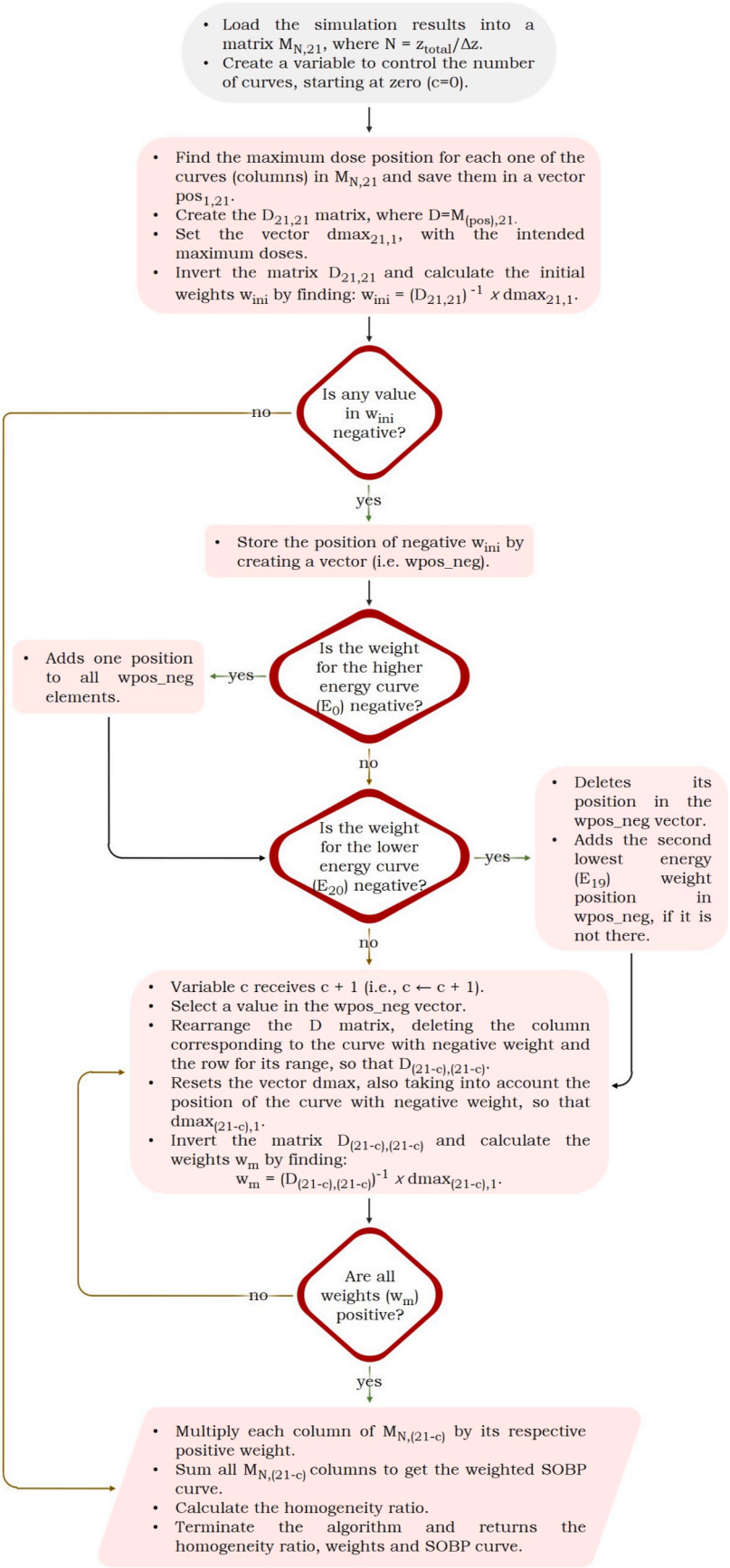

Fig. 5. Flowchart describing the steps involved in the implemented algorithm for computation of the weights and exclusion of the negative ones, acquisition of the homogeneity ratio (*HOM*) and the SOBP curve for the MCMC method.

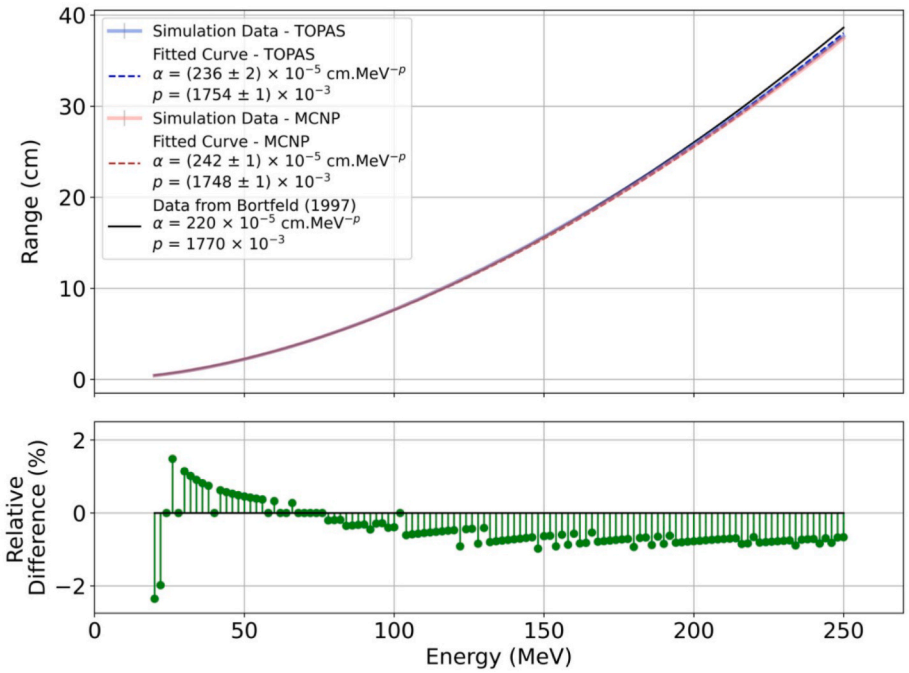

Fig. 6. The upper part of the figure shows data from the TOPAS and MCNP simulations that correlate the beam range to the proton incident energy. These raw data were used to perform a fit following the range-energy relationship, where the parameters α and p were obtained. The same curve is also shown according to the parameter's values from Bortfeld, cited in the literature. The graph at the bottom shows the relative difference, expressed in percentages, between the simulated ranges obtained by MCNP and TOPAS, with the latter adopted as the reference.

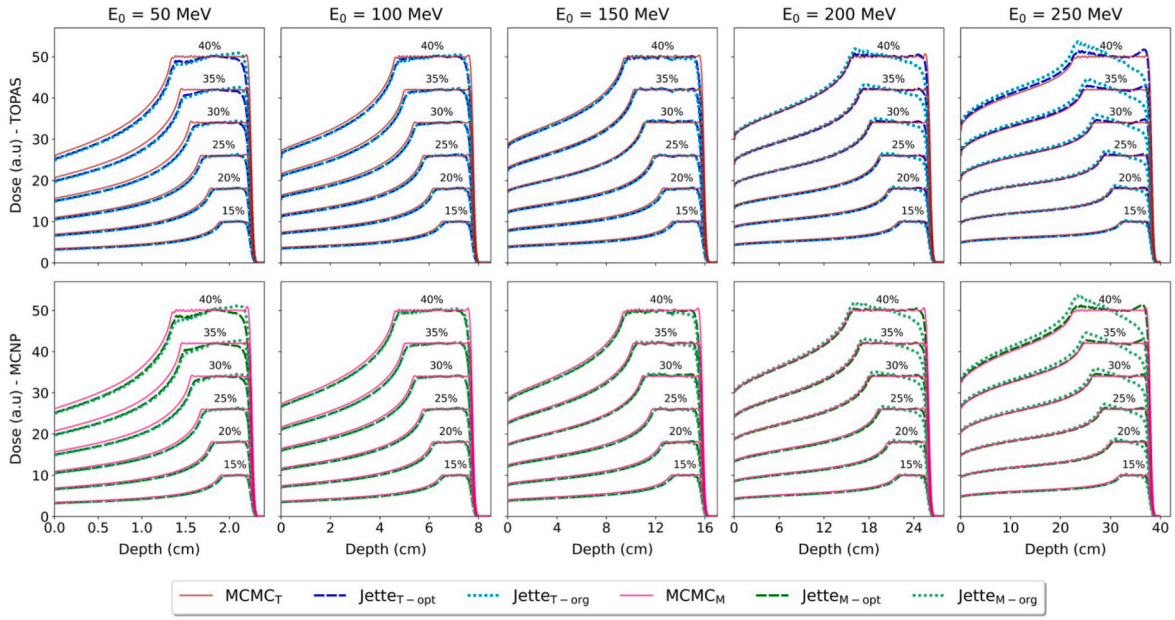

Fig. 7. Design of SOBPs calculated for different widths (χ) and at various depths (i.e., with different E_0) using data simulated with MCNP and TOPAS and by applying different methods for weighting the pristine Bragg curves, these being: MCMC, Jette with p-optimal and Jette with $p = 1.75$ (original).

values obtained are also quite close, showing the largest relative difference of only 2.5% when TOPAS was adopted as reference.

The results show that the p-optimal value varies strongly with the E_0, i.e., the maximum depth of the SOBP and also with its width. Although the analytical method demands the variation of the p -parameter to obtain better *HOM* values, it still retains its merit, as initially stated by Bortfeld and Schlegel (1996), since it allows a fast acquisition of the curve weights. It can be useful in practical applications, for example, to provide an estimation for the immediate entrance dose (Fig. 7). Furthermore, despite the difficulty of defining a unique p-value for insertion into treatment planning systems, the weights obtained can be used as a first guess for iterative computations (Bortfeld and Schlegel, 1996; Jette and Chen, 2011).

After determining the optimal p-values, a comparison was made with previous results of this parameter reported in the literature, for the same maximum incident energy and the same width of the SOBPs, as shown in Fig. 9. It is important to mention that, similarly to this paper, in all studies when the maximum depth of an SOBP increases (i.e., E_0 increases) the p optimal values decrease for all SOBP widths.

The greatest relative differences, displayed in the bar graphs of Fig. 9, occur when comparing the Jette's p-optimal values and those from both codes in this paper. In Jette's paper, 11 pristine Bragg curves ($n = 10$) were adopted to yield the SOBPs, unlike this study that used 21. Based on this, we investigated whether varying the number of Bragg curves used in the production of the SOBPs has an impact on the optimal p-value obtained. The new number of curves adopted was also 11, so

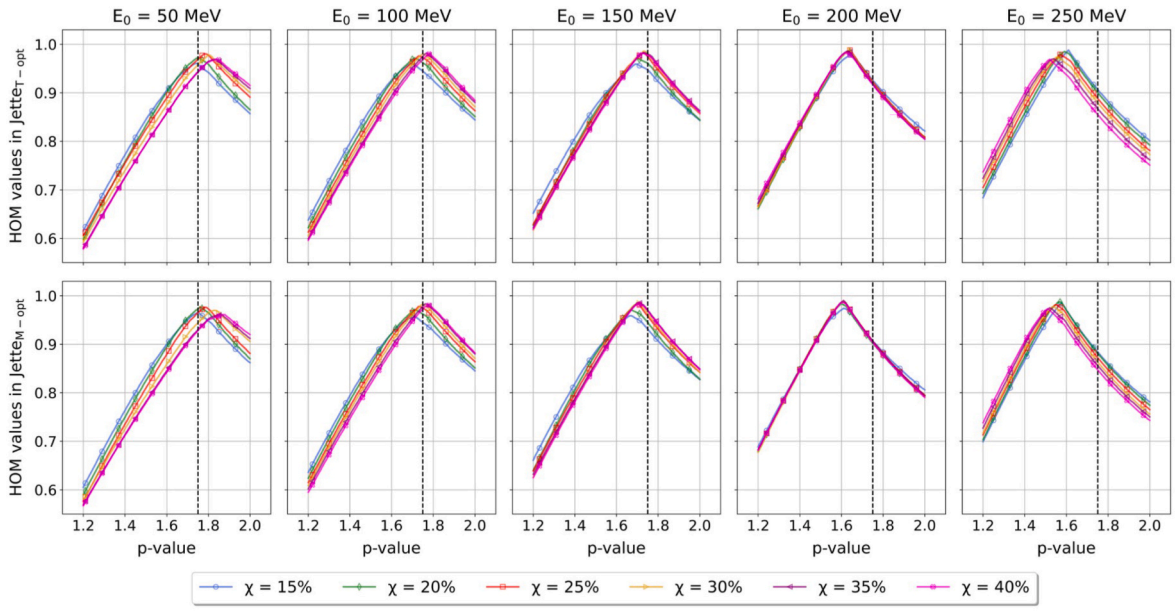

Fig. 8. Dose homogeneity parameter (*HOM*) according to the *p*-values examined for all 30 groups of SOBPs, with six maximum incident energies (E_0) and five distinct widths (χ), for the two MC codes used in this paper. The black dotted line indicates the original *p*-value (1.75) adopted in the first group of simulations (section 3.1).

Table 2
The optimal *p*-values used to create a SOBP with best possible dose homogeneity according to Jette's method. In the second column named 'Code', the letters T and M represent TOPAS and MCNP codes respectively.

χ	Code	Maximum Proton Energies (E_0)				
		50 MeV	100 MeV	150 MeV	200 MeV	250 MeV
15%	T	1.74	1.70	1.69	1.64	1.61
	M	1.75	1.70	1.67	1.61	1.57
20%	T	1.75	1.71	1.70	1.63	1.59
	M	1.76	1.71	1.67	1.60	1.56
25%	T	1.78	1.73	1.73	1.64	1.57
	M	1.78	1.73	1.70	1.61	1.55
30%	T	1.80	1.75	1.73	1.64	1.55
	M	1.83	1.75	1.70	1.61	1.54
35%	T	1.83	1.77	1.73	1.63	1.54
	M	1.86	1.76	1.70	1.61	1.52
40%	T	1.84	1.78	1.72	1.62	1.52
	M	1.87	1.78	1.70	1.60	1.51

that no new simulations were needed. The same algorithm was used to recalculate the weights (Fig. 3) and although the *HOM* values decreased, especially for the larger SOBP widths, the maximum relative difference between the optimized *p*-values with 21 and 11 curves was only up to 2.25% for MCNP and 1.68% for TOPAS (data not shown). Because of these small relative differences, the variation in the number of curves cannot be stated to impact greatly on the obtained optimal *p*-values.

The observed differences between the data from this study and Jette's are presumably due to the different proton cross-section libraries and nuclear interaction physics models. The results of Jette's paper used the LA150 library for proton energies up to 150 MeV and the Bertini/Dresner physics model for higher energies, while this paper employed the default Cascade-Exciton Model (CEM03.03) for basically all energies except those below 1.0 keV, where table-based physics was used (section 2.1.2) (Goorley et al., 2016). A few papers in the literature indicate that using different cross-section tables or physics models for nuclear interactions can lead to large discrepancies between the responses of different codes (Shtejer et al., 2008) or even within the same code (Šolc, 2019). Nevertheless, as in this paper, Titt et al. (2012) has shown that even without detailed selection of any physical parameters, i.e., keeping the default parameters, very similar results can be achieved between different MC codes, such as Geant4 and MCNPX.

The small relative differences shown in Fig. 9 between the *p* -optimal parameters of this paper and those from Velten, could also be attributed to different physics models. The TOPAS version used in this study had as default the *g4em-standard_opt4* physics list that uses the WentzelVI model (Ivanchenko et al., 2010) as well as the Goudsmit-Saunderson model (Goudsmit and Saunderson, 1940a, 1940b) for multiple scattering, whereas the *g4em-standard_opt3*, used by Velten, makes use of the G4UrbanMscModel (Urban, 2002) for multiple scattering of all charged particles.

Furthermore, in both Jette's and Velten's studies, the α and p parameters are cited as equal to that found by Bortfeld ($p = 1.77$ and $\alpha = 0.0022\ \mathrm{cm/MeV}^p$). Thus, the ranges and energies of the pristine Bragg curves could simply have been predicted with small differences tied to these parameters, which may differ from those obtained with the MC codes themselves. It might cause differences in the positions of the SOBPs and the widths, which has already been seen to significantly impact the *p*-optimal values obtained.

3.4. Dose homogeneity parameter -HOM

The dose homogeneity parameters (*HOM*) were obtained for all 30 groups of SOBPs. The pristine Bragg curves of each of the groups, from both MCNP and TOPAS, were weighted according to the different methods considered in this study. The categorization of these analyses is thoroughly outlined in Table 1 and is also employed in Fig. 10 to describe all the *HOM* values resulted from such instances.

Since *HOM* is a ratio between lowest and highest dose within 80% of the SOBP, values close to 1.0 indicate a desirable flatness in this region. The bar graphs of *HOM* values are markedly separated in Fig. 10 by two different methods - Jette's and MCMC. For all groups, the MCMC method created SOBPs with better dose homogeneities when compared to all variations of the Jette's method. This is mainly because Jette's method only allows assigning weights that decrease in value as the incident beam energies that compose the same SOBP decrease, i.e., w_k decreases as E_k. On the other hand, the MCMC method allows to choose the weight values according to the curves' best optimization, regardless of the incident energies, thus enabling a greater flexibility of the algorithm that consequently generates better *HOM* values.

The variation of assigned weights are quite different for the two

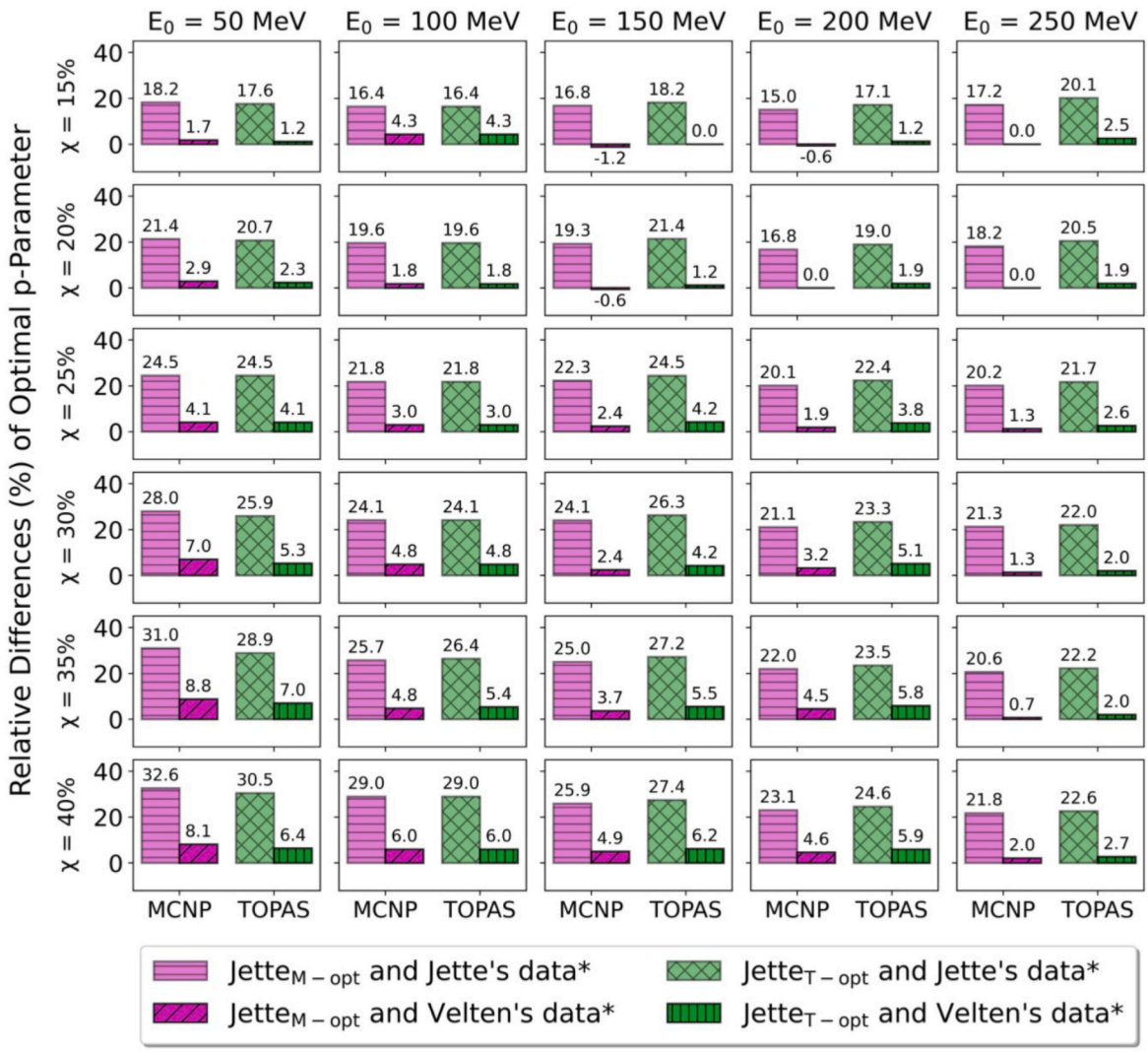

Fig. 9. Relative differences between the *p*-optimal values found in this paper, for the MCNP and TOPAS codes, and those already described in the papers by Jette and Chen (2011) and Velten and Tomé (2020). The differences were sorted according to the maximum incident energy and the SOBP width. The asterisks in the legend denote the data used as reference for the calculations.

methods. For example, in Jette method, the maximum ratio value between the highest and lowest weights is 33.8. This happens for the $\text{Jette}_{\text{M-opt}}$ with SOBP correspondent to $E_0 = 250$ MeV and $\chi = 40\%$. For all instances of this method, the highest and lowest weights match those attributed to the Bragg curves with the highest (E_0) and lowest (E_{20}) energies, respectively. In contrast, for the MCMC method, the maximum ratio value between the highest and lowest weights was obtained from the curves for E_0 and E_2, and is 328.2. This value stands for the MCMC_{T} with SOBP correspondent to $E_0 = 100$ MeV and $\chi = 25\%$, and it emphasizes the versatility of the MCMC method.

Still in Fig. 10, Jette's method shows small differences when comparing *HOM* of SOBPs that used *p*-original value in the calculated weights for TOPAS ($\text{Jette}_{\text{T-org}}$) and MCNP ($\text{Jette}_{\text{M-org}}$). In fact, the weights based on the *p*-original did not vary according to the datasets from the codes used, since they depend only on the *p*-value, set at 1.75, and the number (related to *k* and *n*) of the proton beamlets. This small variation between $\text{Jette}_{\text{T-org}}$ and $\text{Jette}_{\text{M-org}}$ probably happens due to the linear interpolation done with E_k values from TOPAS (from the r_k ranges – Eq. 2) to obtain the incident energies for the SOBPs that were also adopted in MCNP. The evidence of the equality between the weights calculated with original *p* happens when comparing the *HOM* values of $\text{Jette}_{\text{M-org}}$ and $\text{Jette}_{\text{M-Tw-org}}$, since these are exactly the same for all groups.

Still analyzing the *HOM* obtained according to Jette's method with weights calculated using *p*-original, there is a decrease in their value for SOBPs with greater depths (related to E_0) and widths (χ). This is a direct result of the dose tilt, meaning a dose increase at the SOBP's proximal edges compared to the distal ones (see Fig. 7). The *HOM* value related to the lowest E_0 and the larger widths also showed a decrease but now because of slightly higher doses at the SOBP distal portion (described in section 3.2).

The SOBPs weighted by Jette's method, showed significant improvements in *HOM* values when their pairs (MCNP e TOPAS), using computed weights base on *p*-optimal, were compared with those with *p*-original. However, when TOPAS weights with *p*-optimal are applied to the MCNP Bragg curves ($\text{Jette}_{\text{M-Tw-opt}}$), the *HOM* values show a slight decrease or remains the same when compared to $\text{Jette}_{\text{M-opt}}$. The same happens when analyzing only the MCMC method data, the *HOM* values show an overall decrease when comparing $\text{MCMC}_{\text{M-Tw}}$ and MCMC_{M}, indicating that even small differences in the positions of the Bragg curves (seen through Fig. 6) slightly impact on obtaining an ideal SOBP smoothness.

3.5. Gamma analysis

Gamma analyses in 1D were performed so that the full extension of

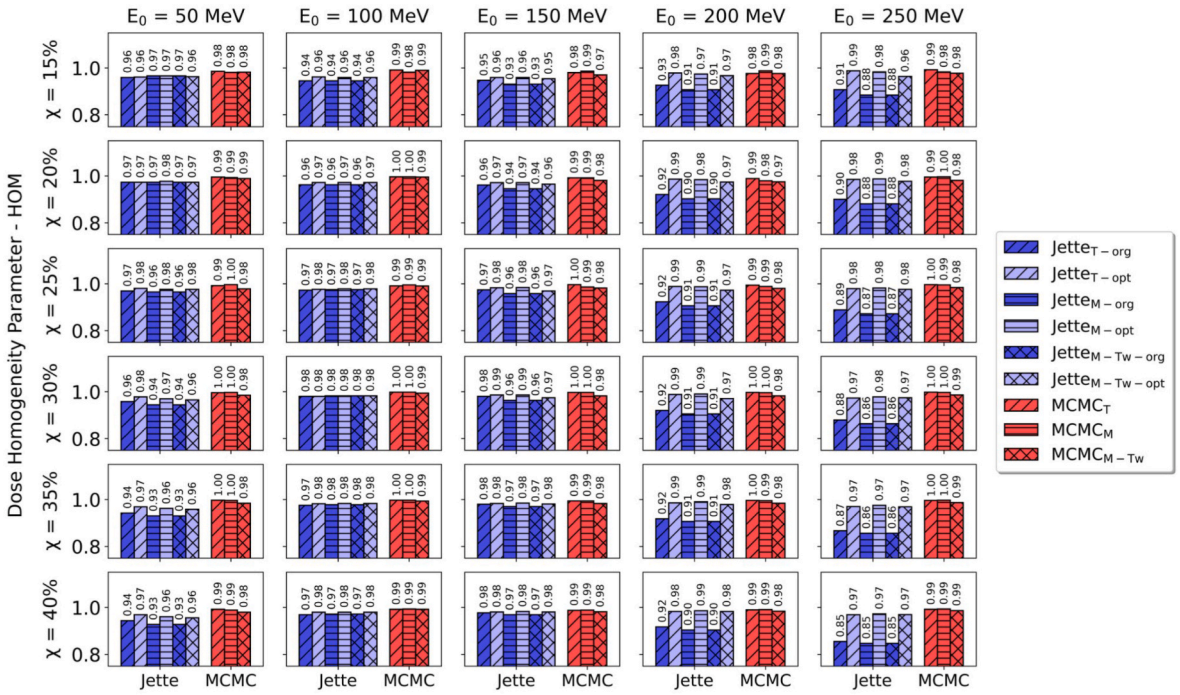

Fig. 10. Dose homogeneity parameter (*HOM*) obtained for each one of the 30 groups of SOBP, classified according to its maximum incident energy and width, considering all investigated methods and MC codes described in Table 1.

the longitudinal dose profiles could be compared for some of the different data sets cited in Table 1. Fig. 11 shows, for each of the 30 groups of SOBPs, gamma analyses between the results of $Jette_{M\text{-}opt}$ and $MCMC_M$ (indicated as A), $Jette_{T\text{-}opt}$ and $MCMC_T$ (B), $Jette_{M\text{-}opt}$ and $Jette_{T\text{-}opt}$ (C), and $MCMC_M$ and $MCMC_T$ (D). Therefore, the first two analyses (A and B) are comparing the methodologies as they use the weighted Bragg curves from the same code to design the SOBPs. In the same way, the last two analyses (C and D) are comparing the codes since

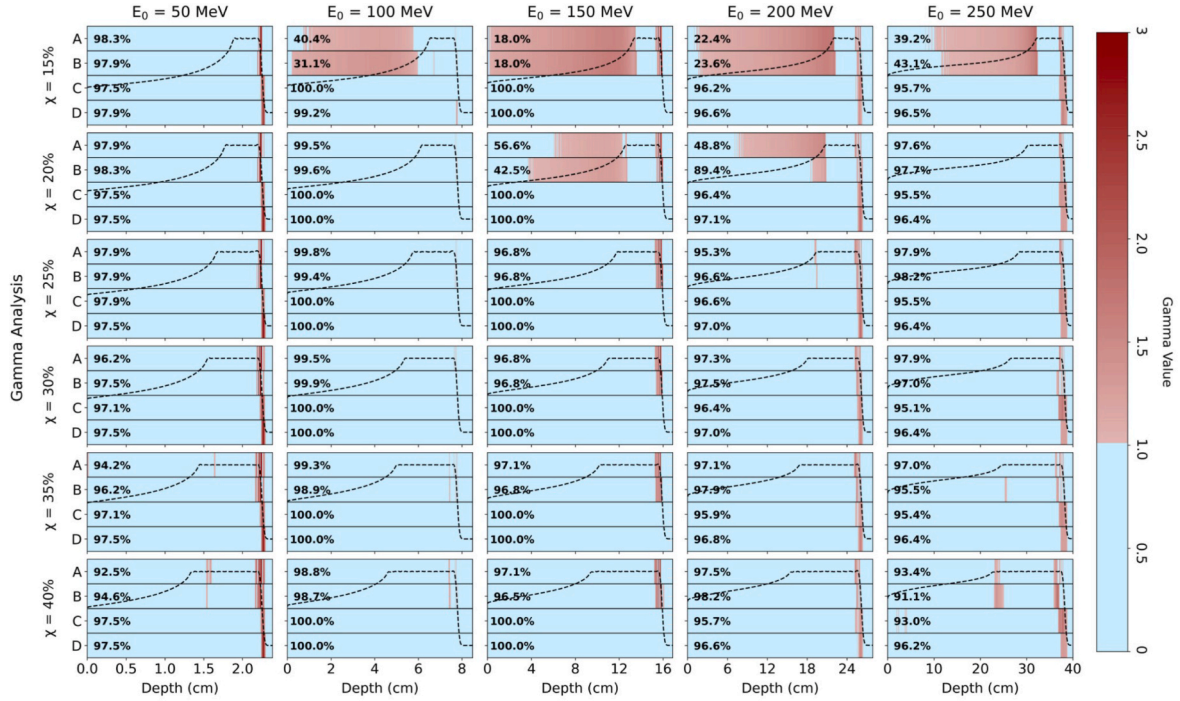

Fig. 11. 1D Gamma analyses of the energy deposition of 30 groups of SOBPs, categorized initially according to their depth (related to E_0) and width (χ). For each group, gamma analyses were performed between the 4 datasets described in Table 1, and are indicated as: **(A)** $Jette_{M\text{-}opt}$ and $MCMC_M$*, **(B)** $Jette_{T\text{-}opt}$ and $MCMC_T$*, **(C)** $Jette_{M\text{-}opt}$ and $Jette_{T\text{-}opt}$*, and **(D)** $MCMC_M$ and $MCMC_T$*. The asterisks here denote the data used as reference for the calculations. The acceptance criteria were 2%/2 mm for all presented data. The red bands correspond to depths with gamma index greater than 1, i.e., points that failed in the test. The percentages denote the number of approved points represented by the blue bands. An SOBP corresponding to the $MCMC_T$ study was placed as an example in each graph (black dashed line) to facilitate the analysis of the corresponding depths.

they keep the same methodology.

The acceptance criteria adopted in the gamma analyses were 2% difference of energy deposition at the middle point of the SOBPs (i.e. at $(1-0.5\chi).R_0$, consistent with the graphs in Fig. 7) and 2 mm distance to agreement for all presented cases (2%/2 mm). In Fig. 11, the red bands correspond to depths where the gamma index was greater than 1, i.e., points which did not meet de gamma criteria and failed in the test, and the blue bands correspond to the points meeting the criteria and passing the test. The percentages values presented in the left sides of each individual graph correspond to the percentage fraction of the dose profile points that met the 2%/2 mm gamma index criterium. A SOBP corresponding to the $MCMC_T$ study was placed as an example in each graph (in black dashed line) only to facilitate the analysis of the corresponding depths.

In general, the regions with the more failing points in the gamma analysis occur when comparing distinct SOBPs weighting methods (Jette and MCMC) for the same MC code (A and B from Fig. 11). This substantial difference in dose deposition, especially for SOBPs with smaller widths ($\chi = 15\%$ and $\chi = 20\%$), highlights that the weights values assigned to the Bragg curves are quite different for these instances, except for the energy of $E_0 = 50$ MeV where we can observe an excellent agreement. Others acceptances criteria have also been tested in the gamma analyses: 2%/3 mm, 3%/2 mm and 3%/3 mm (results not shown). From this, when comparing the 2%/2 mm and 3%/2 mm criteria for example, the points passing the test increase considerably, but not when the 2%/3 mm criteria was applied, confirming the fact that differences in dose deposition are the main cause for the change in acceptance level.

Also, based on these analyses, Jette's SOBPs weights could be able to estimate with some accuracy the entrance dose for SOBPs with widths larger than 20%, since this portion obtained gamma indices below 1.0 for all groups. In further comparison of the different methods, the regions of dose dip resulting from the $Jette_{M\text{-}opt}$ and $Jette_{T\text{-}opt}$ data (see Fig. 7) can explain the differences at the distal and proximal SOBP edges, which are also perceptible for some point in broader widths.

Gamma analysis for the equal SOBP design method (C and D) revealed excellent agreement between the MC codes. The points that failed are at the SOBPs distal edge and belong mainly to the graphs of the highest maximum incident energies (E_0) in all widths. Those failures can be attributed to a combination of factors. Among these factors are the small differences between the ranges of the MCNP and TOPAS curves and the variation of the weight values assigned to the curve with the highest energy (E_0) and the curve with the immediately lower energy (E_1), which directly impact the distal SOBP edge. Also, it is important to note that the weights applied to the Bragg curves were also different within the same method. This occurred because the weights were calculated, by the algorithms represented in Fig. 3 and in Fig. 5, using the results of the TOPAS and MCNP outputs which showed slight differences when compared. Thus, the MCMC method selected the SOBP weights directly based on the outputs results and the Jette method also had its weights calculated according to the selection of a *p*-optimal.

Even with the relative differences of the maximum-to-plateau ratio with both codes reaching 10% for lower energies (result concerning 30 MeV - presented in the discussion of section 3.1), it can be noted that the gamma analyses did not reflect these differences for the SOBPs with a maximum dose of 50 MeV. This is probably because of the compensation for the weights of the Bragg curves to overcome these disparities. Moreover, gamma analysis considers both dose and distance in its calculations, which may be a combination of factors that also do not highlight this difference between the codes and between the methods for lower energies.

Preceding the gamma analyses performed, a gap was visually perceived between the distal edges of the examined SOBPs when comparing both codes. This gap was larger for deeper SOPBs and decreased as it became shallower. Even with the decrease of the gap, for the maximum incident energy of 50 MeV, a high value in the gamma indices for the points that failed the analysis could be noted in most comparisons. In this energy range, the discrepancies may be associated with the sharp-distal falloff, which causes the dose to decrease within a very short distance, leading to large dose differences even for a small gap between the SOBPs analyzed.

4. Conclusion

The pristine Bragg curves obtained from simulations with the MCNP and TOPAS codes made it possible to investigate two different methods for SOBP design - Jette's and MCMC. Initially, values of incident energy of proton beams varying in range were compared for both MC codes and with the literature, exhibiting excellent agreement, with maximum relative differences of only about 2%, and 3.1% respectively.

Thirty variations of SOBPs were created to analyze the different methods, they differed in maximum depths and width. Whilst easily implemented by means of analytical equations, the Jette's method strongly relies on the predefined parameter (*p*-value). The second comparative method, MCMC, offers a more direct approach, requiring only the Bragg curves for each energy used and a filtering of possible negative weights values. The latter method presented smoother SOBPs in immediate results, causing the *HOM* values to be very close to 1.0 for the simulations with both codes, and was executed with less computational time because it did not need the parameters variation related to the weight calculation.

The analyses with Jette's method, instead, permitted the evaluation of various *HOM* values obtained by varying the *p* -parameter for each of the SOBPs. The obtained *p* -optimal values, that produced better *HOM* values, were compared with literature data and showed good agreement with the values described by Velten. Although Jette's method did not produce equally high *HOM* values as the MCMC method, it can be easily used to estimate immediate entrance dose values (for SOBPs broader than 20% of R_0), as well as an initial guess for other iterative methods for computing the SOBP weights.

In addition to the *HOM* values, which analyzes the flatness of SOBPs within 80% of their extent, gamma analyses were performed in order to cross-check results along the entire dose deposition extent, analyzing SOBPs from different weighting methods and MC codes. The HOM parameter proved important because it allowed an evaluation of the flatness of the SOBPs independent of other comparisons. Gamma analysis, on the other hand, allowed to reveal differences in portions of the entrance doses when using different SOBPs weighting methods and differences between the distal and proximal edges in several cases.

Even without the selection of complex physics simulation parameters (i.e., using most of them as defaults), it was possible to obtain a good concordance for simulation results with TOPAS and MCNP codes. This was reflected in both range-energy relationships and using the two tools (HOM and gamma analysis) to compare the results for the SOBPs obtained with the same weighting method.

The algorithms presented in this paper, which contain step-by-step development of the weighting methods used, are simple enough and allowed SOBP construction in hundredths of seconds when run on a domestic computer. From the methods and analysis, it is also possible to use any pristine Bragg curve dataset for new SOBP designs and trials. Furthermore, the p-optimized results obtained allows a feasible start for iterative calculations of SOBPs weights, as well as obtaining an estimate of the entrance dose for the cases studied.

Author statement

I. S. L. Branco: Conceptualization, Methodology, Software, Formal analysis, Investigation, Writing - Original Draft, Writing - Review & Editing. **A. L. Burin:** Conceptualization, Investigation. **J. J. N. Pereira:** Conceptualization, Investigation. **P. T. D. Siqueira:** Formal analysis, Validation. **J. M. B. Shorto:** Formal analysis, Validation. **H. Yoriyaz:** Conceptualization, Methodology, Formal analysis, Investigation,

Writing - Original Draft, Supervision.

Declaration of competing interest

The authors declare the following financial interests/personal relationships which may be considered as potential competing interests.

I. S. L. Branco received financial support from Conselho Nacional de Desenvolvimento Científico e Tecnológico - CNPq (public funding scholarship - government agency). A. L. Burin received financial support from Coordenação de Aperfeiçoamento de Pessoal de Nível Superior - CAPES (public funding scholarship - government agency). J. J. N. Pereira received financial support from Coordenação de Aperfeiçoamento de Pessoal de Nível Superior - CAPES (public funding scholarship - government agency).

Data availability

Data will be made available on request.

Acknowledgments

The authors gratefully acknowledge the financial support from the funding agencies *Conselho Nacional de Desenvolvimento Científico e Tecnológico* - CNPq (protocol 168933/2018–7) and *Coordenação de Aperfeiçoamento de Pessoal de Nível Superior* - CAPES (protocols 88887.506528/2020–00 and 88887.704665/2022–00).

References

Agostinelli, S., Allison, J., Amako, K., et al., 2003. Geant4—a simulation toolkit. Nucl. Instrum. Methods Phys. Res. 506, 250–303. https://doi.org/10.1016/S0168-9002(03)01368-8.

Allison, J., Amako, K., Apostolakis, J., et al., 2016. Recent developments in Geant4. Nucl. Instrum. Methods Phys. Res. 835, 186–225. https://doi.org/10.1016/j.nima.2016.06.125.

Bortfeld, T., 1997. An analytical approximation of the Bragg curve for therapeutic proton beams. Med. Phys. 24, 2024–2033. https://doi.org/10.1118/1.598116.

Bortfeld, T., Schlegel, W., 1996. An analytical approximation of depth - dose distributions for therapeutic proton beams. Phys. Med. Biol. 41, 1331–1339. https://doi.org/10.1088/0031-9155/41/8/006.

Evans, R.D., 1955. The Atomic Nucleus. McGraw-Hill, New York.

Gardey, K.-U., Oelfke, U., Lam, G.K.Y., 1999. Range modulation in proton therapy - an optimization technique for clinical and experimental applications. Phys. Med. Biol. 44, N81–N88. https://doi.org/10.1088/0031-9155/44/6/402.

Ghorbani, M., Jia, S.B., Khosroabadi, M., et al., 2017. Evaluation of the effect of soft tissue composition on the characteristics of spread-out Bragg peak in proton therapy. J. Cancer Res. Therapeut. 13, 974. https://doi.org/10.4103/0973-1482.220420.

Golub, G.H., Reinsch, C., 1971. Singular value decomposition and least squares solutions. In: Linear Algebra. Springer, pp. 134–151.

Goorley, T., James, M., Booth, T., et al., 2016. Features of MCNP6. Ann. Nucl. Energy 87, 772–783. https://doi.org/10.1016/j.anucene.2015.02.020.

Goudsmit, S., Saunderson, J.L., 1940a. Multiple scattering of electrons. II. Phys. Rev. 58, 36–42. https://doi.org/10.1103/PhysRev.58.36.

Goudsmit, S., Saunderson, J.L., 1940b. Multiple scattering of electrons. Phys. Rev. 57, 24–29. https://doi.org/10.1103/PhysRev.57.24.

Hérault, J., Iborra, N., Serrano, B., et al., 2007. Spread-out Bragg peak and monitor units calculation with the Monte Carlo Code MCNPX. Med. Phys. 34, 680–688. https://doi.org/10.1118/1.2431473.

Hérault, J., Iborra, N., Serrano, B., et al., 2005. Monte Carlo simulation of a protontherapy platform devoted to ocular melanoma. Med. Phys. 32, 910–919. https://doi.org/10.1118/1.1871392.

Ivanchenko, V.N., Kadri, O., Maire, M., et al., 2010. Geant4 models for simulation of multiple scattering. J Phys Conf Ser 219, 032045. https://doi.org/10.1088/1742-6596/219/3/032045.

James, S.S., Grassberger, C., Lu, H.-M., 2018. Considerations when treating lung cancer with passive scatter or active scanning proton therapy. Transl. Lung Cancer Res. 7, 210. https://doi.org/10.21037/tlcr.2018.04.01.

Jarlskog, C.Z., Paganetti, H., 2008. Physics settings for using the Geant4 toolkit in proton therapy. IEEE Trans. Nucl. Sci. 55, 1018–1025. https://doi.org/10.1109/TNS.2008.922816.

Jette, D., Chen, W., 2011. Creating a spread-out Bragg peak in proton beams. Phys. Med. Biol. 56, N131–N138. https://doi.org/10.1088/0031-9155/56/11/N01.

Lomax, A., 1999. Intensity modulation methods for proton radiotherapy. Phys. Med. Biol. 44, 185–205. https://doi.org/10.1088/0031-9155/44/1/014.

Moskvin, V.P., Estabrook, N.C., Cheng, C.-W., et al., 2015. Effect of scanning beam for superficial dose in proton therapy. Technol. Cancer Res. Treat. 14, 643–652. https://doi.org/10.7785/tcrt.2012.500435.

Newhauser, W.D., Zhang, R., 2015. The physics of proton therapy. Phys. Med. Biol. 60, R155–R209. https://doi.org/10.1088/0031-9155/60/8/R155.

Paganetti, H., 2018. Proton Therapy Physics, second ed. CRC Press.

Pedroni, E., Scheib, S., Böhringer, T., et al., 2005. Experimental characterization and physical modelling of the dose distribution of scanned proton pencil beams. Phys. Med. Biol. 50, 541–561. https://doi.org/10.1088/0031-9155/50/3/011.

Pelowitz, D.B., 2013. MCNP6 User's Manual. LA-CP-13-00634, version 1.0.

Pelowitz, D.B., 2008. MCNPX User's Manual, Version 2.6. 0, LA-CP-07-1473. Los Alamos National Laboratory, Los Alamos (NM).

Perl, J., Shin, J., Schümann, J., et al., 2012. TOPAS: an innovative proton Monte Carlo platform for research and clinical applications. Med. Phys. 39, 6818–6837. https://doi.org/10.1118/1.4758060.

Rezaee, L., 2018. Design of spread-out Bragg peaks in hadron therapy with oxygen ions. Rep. Practical Oncol. Radiother. 23, 433–441. https://doi.org/10.1016/j.rpor.2018.08.004.

Rossum, G. van, 1995. Python Tutorial: Technical Report CS-R9526. Centrum voor Wiskunde en Informatica, Amsterdam.

Sawakuchi, G.O., Titt, U., Mirkovic, D., et al., 2008. Density heterogeneities and the influence of multiple Coulomb and nuclear scatterings on the Bragg peak distal edge of proton therapy beams. Phys. Med. Biol. 53, 4605–4619. https://doi.org/10.1088/0031-9155/53/17/010.

Shtejer, K., Arruda-Neto, J.D.T., Schulte, R., et al., 2008. Comparison of MCNPX and GEANT4 to predict the contribution of non-elastic nuclear interactions to absorbed dose in water, PMMA and A150. In: AIP Conference Proceedings. American Institute of Physics, pp. 136–140.

Šolc, J., 2019. Comparison of proton interaction physics models and cross section libraries for proton therapy Monte Carlo simulations by MCNP6.2 code. Radiat. Meas. 125, 57–68. https://doi.org/10.1016/j.radmeas.2019.04.016.

Testa, M., Min, C.H., Verburg, J.M., et al., 2014. Range verification of passively scattered proton beams based on prompt gamma time patterns. Phys. Med. Biol. 59, 4181–4195. https://doi.org/10.1088/0031-9155/59/15/4181.

Testa, M., Schümann, J., Lu, H.-M., et al., 2013. Experimental validation of the TOPAS Monte Carlo system for passive scattering proton therapy. Med. Phys. 40, 121719 https://doi.org/10.1118/1.4828781.

Titt, U., Bednarz, B., Paganetti, H., 2012. Comparison of MCNPX and Geant4 proton energy deposition predictions for clinical use. Phys. Med. Biol. 57, 6381.

Ulmer, W., 2007. Theoretical aspects of energy–range relations, stopping power and energy straggling of protons. Radiat. Phys. Chem. 76, 1089–1107. https://doi.org/10.1016/j.radphyschem.2007.02.083.

Urban, L., 2002. Multiple Scattering Model in Geant4.

Velten, C., Tomé, W.A., 2020. Simulation of spread-out bragg peaks in proton beams using Geant4/TOPAS. Biomed Phys Eng Express 6, 047001. https://doi.org/10.1088/2057-1976/ab8f6d.

Virtanen, P., Gommers, R., Oliphant, T.E., et al., 2020. SciPy 1.0: fundamental algorithms for scientific computing in Python. Nat. Methods 17, 261–272. https://doi.org/10.1038/s41592-019-0686-2.

Yokokawa, K., Furusaka, M., Matsuura, T., et al., 2019. A new SOBP-formation method by superposing specially shaped Bragg curves formed by a mini-ridge filter for spot scanning in proton beam therapy. Phys. Med. 67, 70–76. https://doi.org/10.1016/j.ejmp.2019.10.036.

Zieb, K., Hughes, H.G., James, M.R., et al., 2018. Review of heavy charged particle transport in MCNP6.2. Nucl. Instrum. Methods Phys. Res. 886, 77–87. https://doi.org/10.1016/j.nima.2018.01.002.